Materials Transactions, Vol. 46, No. 6 (2005) pp. 1180 to 1186
Special Issue on Computer Modeling of Materials and Processes

Glass Transition within Cluster Variation and Path Probability Methods

Tetsuo Mohri

Division of Materials Science and Engineering, Graduate School of Engineering, Hokkaido University, Sapporo 060-8628 Japan

Thermodynamic framework of Crystal-Glass transition is described within the Cluster Variation Method (CVM). Free energy is calculated as a function of order parameter at various temperatures and T_0 diagram is obtained. It is demonstrated that the glass transition temperature can be interpreted as the spinodal ordering temperature in the order-disorder transition. The advantage of the present description is that the kinetic behavior can be investigated within the same framework by employing Path Probability Method (PPM). Therefore, the combination of the CVM and PPM provides a unique theoretical tool to study Crystal-Glass transition in a consistent manner covering thermodynamics and kinetics.

(Received December 22, 2004; Accepted February 15, 2005; Published June 15, 2005)

Keywords: *glass transition, cluster variation method, path probability method, T_0-diagram, first order transition*

1. Introduction

Bulk Metallic Glasses (BMG) have been attracting broad attentions for their superior mechanical, magnetic and corrosion properties. The bulk of the investigation, however, has been directed towards the development and applications of new BMG's, and the understanding of fundamental properties of BMG is still far from satisfactory. In particular, the studies of thermodynamic stability and its structure correlation leave numerous subjects un-clarified. Since unique properties of BMG are exclusively owing to Crystal-Glass (CG) transition, fundamental studies of BMG and CG transitions are inseparable. Recalling that CG transition is not a fully equilibrium transition, a successful theory of CG transition should be capable of covering both thermodynamics and kinetics aspects in a consistent manner.

Cluster Variation Method (CVM)[1] has been recognized as one of the most reliable theoretical tools to investigate order-disorder transition. Path Probability Method[2] which is the natural extension of the CVM to time domain clarifies various temporal behavior in the atomistic level. Then, the combination of the CVM and PPM is best suited to investigate the order-disorder transition from non-equilibrium to equilibrium states. The limitation of the conventional CVM, however, is the fact that only uniform deformation of the system is allowed and no local displacement can be introduced. On the other hand, recent development of Continuous Displacement Cluster Variation Method (CDCVM)[3–8] lifts such a limitation and opens up a possibility of investigating a topologically disordered structure in addition to substitutionaly disordered phase. The investigation of thermodynamic stability of the BMG which forms non-Bravais lattice is, therefore, a potential candidate for the application of CDCVM.

Yet the thermodynamic framework of CG transition has not been described within the conventional CVM, and it is deemed indispensable to examine the capability of describing the essential thermodynamic feature of CG transition prior to the application of the CDCVM. Motivated by the excellent article of Okamoto *et al.*,[9] the main objectives of the present study is to describe the thermodynamic frameworks of CG transition based on CVM and to clarify kinetic aspects by Path Probability Method (PPM). Thereby, a unified interpretation of CG transition covering both thermodynamics and kinetics is attempted. The organization of the present work is as follows. In the next section, essential aspects of CVM and PPM are summarized. In the third section, independent configurational variables are introduced to correlate order-disorder transition with CG transition. Main results are presented in the last section and discussion follows.

2. Cluster Variation Method and Path Probability Method

CVM was devised by Kikuchi originally as a statistical mechanics methods to study interacting particles. It was van Baal[10] who first applied the CVM to the calculation of a phase diagram. Then, Kikuchi and de Fontaine[11,12] demonstrated that the Cu–Au type phase diagram was reproduced much more accurately as compared with the one[13] obtained based on the traditional Bragg-Williams (BW) approximation.[14] The advantage of the CVM over the BW approximation is addressed not only in terms of the topology of the resultant phase boundaries but also the accuracy of the order of transition. In fact, BW approximation fails to reproduce the first-order nature of the $L1_0$-disorder transition at 1:1 stoichiometirc composition, while the CVM yields the correct order of the transition.

The advantage of the CVM is the fact that CVM is able to incorporate wide range of atomic correlations which play a significant role especially at the phase transition. The range of the correlation is characterized by the largest cluster involved in the entropy formula which is termed *basic cluster* and specifies the level of the approximation. For the Bragg-Williams approximation, a lattice point is the basic cluster and it is often called point approximation in the CVM hierarchy.

Within the *tetrahedron* approximation,[15] for instance, the largest cluster is the nearest neighbor tetrahedron cluster and the entropy for a fcc disorderd phase is written as

$$S_T^{\mathrm{dis}} = k_{\mathrm{B}} \cdot \ln \frac{\left\{\prod_{i,j}(Ny_{ij})!\right\}^6 \cdot (N!)}{\left\{\prod_i (Nx_i)!\right\}^5 \cdot \left\{\prod_{i,j,k,l}(Nw_{ijkl})!\right\}^2} \qquad (1)$$

where k_{B} is the Boltzmann constant, N is the number of

lattice point, and x_i, y_{ij} and w_{ijkl} are cluster probabilities of finding an atomic arrangement specified by subscript(s) on a lattice point, pair and tetrahedron clusters. This is the most often employed approximation in the CVM and even first-principles calculations by combining with electronic structure calculations can be performed[16–19] within this approximation. For an ordered phase, one needs to distinguish sublattices and the exponents of the entropy formula are modified depending upon the phase of interest. For the $L1_0$ ordered phase which is the main concern of the present study, the entropy formula is given as

$$S_T^{L1_0} = k_B \cdot \ln \frac{\left\{\prod_{i,j}(Ny_{ij}^{\alpha\alpha})!\right\}\left\{\prod_{i,j}(Ny_{ij}^{\alpha\beta})!\right\}^4\left\{\prod_{i,j}(Ny_{ij}^{\beta\beta})!\right\}N!}{\left\{\prod_i(Nx_i^{\alpha})!\right\}^{5/2}\left\{\prod_i(Nx_i^{\beta})!\right\}^{5/2}\left\{\prod_{i,j,k,l}(Nw_{ijkl}^{\alpha\alpha\beta\beta})!\right\}^2} \tag{2}$$

where the superscripts α and β specify the sublattices. It is noted that the disordered phase is a limiting case where the distinction of the sublattices in an ordered phase vanishes. This can be easily seen that the sum of the exponents in eq. (2) is identical to the one for each cluster probability in eq. (1). In the following discussions, we focus only on $L1_0$ ordered phase.

In order to describe the free energy, a nearest neighbor pair interaction model is applied for the internal energy E which is given by

$$E^{L1_0} = \frac{1}{2} \cdot N \cdot \sum_{i,j} e_{ij} \cdot (y_{ij}^{\alpha\alpha} + 4y_{ij}^{\alpha\beta} + y_{ij}^{\beta\beta}) \tag{3}$$

where e_{ij} is the atomic pair interaction energy between species i and j and the coefficient of the cluster probability describes the degeneracy of each pair in the $L1_0$ ordered phase. It is noted that the range of atomic correlation generally exceeds the one for atomic interaction, hence the largest cluster in the internal energy term should be included in the basic cluster in the entropy formula. This criterion is certainly satisfied in the present study, *i.e.* $y_{ij} \in w_{ijkl}$.

By combining eqs. (2) and (3), the free energies of an $L1_0$ ordered phase is obtained as

$$\begin{aligned} F^{L1_0} = {} & \frac{1}{2} \cdot N \cdot \sum_{i,j} e_{ij} \cdot (y_{ij}^{\alpha\alpha} + 4y_{ij}^{\alpha\beta} + y_{ij}^{\beta\beta}) \\ & - k_B T \cdot \ln \frac{\left\{\prod_{i,j}(Ny_{ij}^{\alpha\alpha})!\right\}\left\{\prod_{i,j}(Ny_{ij}^{\alpha\beta})!\right\}^4\left\{\prod_{i,j}(Ny_{ij}^{\beta\beta})!\right\}N!}{\left\{\prod_i(Nx_i^{\alpha})!\right\}^{5/2}\left\{\prod_i(Nx_i^{\beta})!\right\}^{5/2}\left\{\prod_{i,j,k,l}(Nw_{ijkl}^{\alpha\alpha\beta\beta})!\right\}^2}. \end{aligned} \tag{4}$$

The equilibrium state is determined by minimizing the free energy with respect to the cluster probabilities,

$$\frac{\partial F^{L1_0}}{\partial \phi_{ij\ldots}^{\gamma\delta\ldots}} = 0 \tag{5}$$

where ϕ represents a cluster probability and the subscripts and superscripts denote the atomic configuration and the sublattices, respectively.

Path Probability Method (PPM) was devised as the natural extension of the CVM to time domain by Kikuchi. The time evolution of each cluster probability is described by the *path variable* which constitutes *Path Probability Function, P*, which is a counter part of the free energy of the CVM and is given as a product of the following three terms,

$$P_1 = \prod_{\delta=\alpha}^{\beta} (\theta \cdot \Delta t)^{\frac{N}{2} \cdot X_{1,\bar{1}}^{\delta,\delta}} (\theta \cdot \Delta t)^{\frac{N}{2} \cdot X_{1,1}^{\delta,\delta}} (1 - \theta \cdot \Delta t)^{\frac{N}{2} \cdot X_{1,1}^{\delta,\delta}} (1 - \theta \cdot \Delta t)^{\frac{N}{2} \cdot X_{1,\bar{1}}^{\delta,\delta}} \tag{6}$$

$$P_2 = \exp\left(-\frac{\Delta E}{2k_B T}\right), \tag{7}$$

and

$$P_3 = k_B \cdot \ln \frac{\left\{\prod_{i,j}(NY_{ij,kl}^{\alpha\alpha})!\right\}\left\{\prod_{i,j}(NY_{ij,kl}^{\alpha\beta})!\right\}^4\left\{\prod_{i,j}(NY_{ij,kl}^{\beta\beta})!\right\}N!}{\left\{\prod_i(NX_{i,j}^{\alpha})!\right\}^{5/2}\left\{\prod_i(NX_{i,j}^{\beta})!\right\}^{5/2}\left\{\prod_{i,j,k,l}(NW_{ijkl,mnop}^{\alpha\alpha\beta\beta})!\right\}^2} \tag{8}$$

where θ is the spin flipping probability per unit time that corresponds to the diffusivity of an alloy system, and ΔE is the change of the internal energy during Δt given by

$$\Delta E = \frac{1}{2} \cdot N \cdot \sum_{\gamma,\delta} \omega^{\gamma\delta} \sum_{i,j} e_{ij} \cdot \{y_{ij}^{\gamma\delta}(t + \Delta t) - y_{ij}^{\gamma\delta}(t)\} \tag{9}$$

where $\omega^{\gamma\delta}$ is the degeneracy factor of each pair which is equivalent to the coefficient of pair probability in eq. (3). $X_{i,j}$, $Y_{ij,kl}$ and $W_{ijkl,mnop}$ are path variables for point, pair and tetrahedron clusters, which describe the time transition of the species on the sublattices specified in the sub- and superscripts, respectively. These are the key variables correspond-

ing to cluster probabilities of the CVM.

It may be easier to grasp the physical meaning of a path variable by exemplifying a simple point cluster. The first subscript i in $X^{\alpha}_{i,j}$ indicates the configuration on a point cluster at time t, while the second subscript j indicates the one at time $t+\Delta t$, and the cluster probability x^{α}_1 at time t can be written as,

$$x^{\alpha}_1(t) = X^{\alpha}_{1,1}(t, t+\Delta t) + X^{\alpha}_{1,\bar{1}}(t, t+\Delta t). \tag{10}$$

Note that 1 and $\bar{1}(-1)$ in the subscript indicate A and B atoms, respectively, throughout this study. Likewise, the cluster probability x^{α}_1 at time $t+\Delta t$ can be written as

$$x^{\alpha}_1(t+\Delta t) = X^{\alpha}_{1,1}(t, t+\Delta t) + X^{\alpha}_{\bar{1},1}(t, t+\Delta t). \tag{11}$$

It is noticed that these are generalized geometrical conditions in the time-space which will be introduced soon. One can easily extend the relationships to the time evolution of the pair configuration as follows,

$$\begin{aligned} y^{\gamma\delta}_{1,1}(t) = {} & Y^{\gamma\delta}_{11,11}(t, t+\Delta t) + Y^{\gamma\delta}_{11,\bar{1}\bar{1}}(t, t+\Delta t) \\ & + Y^{\gamma\delta}_{11,1\bar{1}}(t, t+\Delta t) \end{aligned} \tag{12}$$

and

$$\begin{aligned} y^{\gamma\delta}_{1,1}(t+\Delta t) = {} & Y^{\gamma\delta}_{11,11}(t, t+\Delta t) + Y^{\gamma\delta}_{1\bar{1},11}(t, t+\Delta t) \\ & + Y^{\gamma\delta}_{\bar{1}1,11}(t, t+\Delta t) \end{aligned} \tag{13}$$

P_1 in eq. (6) describes the non-correlated spin flipping events over an entire lattice point and P_2 in eq. (7) suggests the probability of gaining the thermal activation energy ΔE by a system interacting with a heat reservoir. The characteristic feature of the PPM is written in the third term, P_3, which is quite similar to the entropy term of the CVM given in eq. (2). In fact, P_3 describes the microscopic freedom of atomic transition paths, which is the extension of the configurational freedom in the lattice written in the entropy term. Such a parallel formalism with the CVM is the natural consequence of the PPM devised as the extension of the CVM to the time domain.

The key criterion claimed in the PPM is that the most probable transition path is determined so that the PPF is maximized with respect to the path variables,

$$\frac{\partial P}{\partial \Xi^{\{\alpha\beta\ldots\},\{\gamma\delta\ldots\}}_{\{ij\ldots\},\{kl\ldots\}}} = 0 \tag{14}$$

where P is the PPF given by

$$P = P_1 \cdot P_2 \cdot P_3 \tag{15}$$

and $\Xi^{\{\alpha\alpha\ldots\},\{\gamma\delta\ldots\}}_{\{ij\ldots\},\{kl\ldots\}}$ indicates a path variable describing the transition from $\{ij\ldots\}$ to $\{kl\ldots\}$ during the infinitesimal time step Δt. This condition is the counterpart of the minimization condition of the free energy of the CVM given in eq. (5).

Two points should be addressed. One is that, unlike other kinetic theories, PPM does not explicitly deal with the free energy or its derivative. This is a unique feature of the PPM and ensures the applicability of the PPM even for a *far-from-equilibrium* transition.[20–26] The second point is that the present formulae given by eqs. (6)–(8) are applicable only to a spin kinetics.[32] Although more appropriate for an alloy system are the exchange kinetics[33] or vacancy mediated kinetics, those kinetics demand formidably many microscopic paths and the formulation as well as numerical calculation become intractable. A critical deficiency of the spin kinetics when dealing with an alloy originates from the fact that the species is not conserved with time. However, at 1:1 stoichiometric composition, it can be shown that the conservation of the spin species is observed without any additional constraints. Hence, the present calculation confined to 1:1 stoichiometric composition simulates an alloy system.

3. Correlation Functions and Constrained Minimization

As was seen in the previous section, the cluster probabilities are the key quantities in both equilibrium and kinetics analysis. However, cluster probabilities are related through

$$\sum_i x^{\gamma}_i = \sum_{i,j} y^{\gamma\delta}_{ij} = \sum_{i,j,k,l} w^{\alpha\alpha\beta\beta}_{ijkl} = \cdots\cdots = 1 \tag{16}$$

and

$$x^{\alpha}_i = \sum_{\gamma}\sum_{j} y^{\alpha\gamma}_{ij} = \sum_{j,k,l} w^{\alpha\alpha\beta\beta}_{ijkl} \tag{17}$$

which are known as normalization condition and geometrical conditions, respectively. Therefore, cluster probabilities in the free energy in eq. (4) are not mutually independent, and in terms of mathematical transparency, it is more convenient to work with independent variables. Hence, the correlation functions[27,28] are introduced in the following way.

The correlation function ξ_J for a J-point cluster is defined as the ensemble average of a product of spin variables $\langle\sigma_1 \cdot \sigma_2 \cdots \sigma_p \cdots \sigma_J\rangle$, where σ_p is the *spin variable* which takes either $+1$ or -1 depending upon A or B atom located at the lattice point p. It has been shown that a cluster probability $X_{\{J\}}(l)$ of which configuration is specified by l can be given by a liner transformation of a set of correlation functions,

$$X_{\{J\}}(l) = \frac{1}{2^{n_e}}\left\{1 + \sum_{l'} V_{\{J\}}(l, l') \cdot \xi_{l'}\right\} \tag{18}$$

where V is called V-matrix[27,28] and involves the sum of products of $i, j, k\ldots$, and l' suggests a sub-cluster contained in the cluster l. Since mathematical details have been amply demonstrated,[27,28] we simply reproduce the specific examples for a point, pair and tetrahedron clusters as follows,

$$x_i = \frac{1}{2}(1 + i \cdot \xi_1) \tag{19}$$

$$y_{ij} = \frac{1}{2^2}\{1 + (i+j)\cdot\xi_1 + i\cdot j\cdot\xi_2\} \tag{20}$$

and

$$\begin{aligned} w_{ijkl} = {} & \frac{1}{2^4}\{1 + (i+j+k+l)\cdot\xi_1(ij+ik+il+\cdots+kl) \\ & \cdot\xi_2 + (ijk+\cdots+jkl)\cdot\xi_3 + ijkl\cdot\xi_4\}. \end{aligned} \tag{21}$$

It is noticed that the above discussions and formulae given in eqs. (18)–(21) are limited to a disordered phase. For an ordered phase, one needs to distinguish sub-lattices. The extension is quite straightforward and eqs. (19) and (20), for instance, can be rewritten as,

$$x_i^\delta = \frac{1}{2}(1 + i \cdot \xi_1^\delta) \tag{22}$$

and

$$y_{ij}^{\gamma\delta} = \frac{1}{2^2}\{1 + i \cdot \xi_1^\gamma + j \cdot \xi_1^\delta + i \cdot j \cdot \xi_2^{\gamma\delta}\}. \tag{23}$$

Then, the free energy of an $L1_0$ ordered phase given in eq. (4) is rewritten as

$$\begin{aligned} F^{L1_0} &= F(T, \{e_{ij}\}; x_i^\alpha, x_i^\beta, y_{ij}^{\alpha\alpha}, y_{ij}^{\alpha\beta}, y_{ij}^{\beta\beta}, w_{ijkl}^{\alpha\alpha\beta\beta}) \\ &= \hat{F}^{L1_0}(T, \{e_{ij}\}; = \xi_1^\alpha, \xi_1^\beta, \xi_2^{\alpha\alpha}, \xi_2^{\alpha\beta}, \xi_2^{\beta\beta}, \xi_3^{\alpha\alpha\beta}, \xi_3^{\alpha\beta\beta}, \xi_4^{\alpha\alpha\beta\beta}). \end{aligned} \tag{24}$$

Since the atomic interaction energies $\{e_{ij}\}$ are kept to be constant, they are omitted from the free energy in the following descriptions. Temperature T in the present study is normalized with respect to effective pair interaction energy defined as,

$$v_2 = \frac{(e_{AA} + e_{BB})}{2} - e_{AB} \tag{25}$$

and is given by

$$T^* = \frac{k_B \cdot T}{v_2}. \tag{26}$$

Then, the free energy of an $L1_0$ ordered phase is symbolically expressed as

$$F^{L1_0} = F(T^*, \xi_1^\alpha, \xi_1^\beta, \xi_2^{\alpha\alpha}, \xi_2^{\alpha\beta}, \xi_2^{\beta\beta}, \xi_3^{\alpha\alpha\beta}, \xi_3^{\alpha\beta\beta}, \xi_4^{\alpha\alpha\beta\beta}), \tag{27}$$

where $\hat{F}^{L1_0}$ is replaced by F^{L1_0} for the sake of convenience. When our discussion is confined to a fixed 1:1 stoichiometry, which was required by PPM calculations for a spin kinetics, the number of independent correlation functions are reduced due to the symmetry of the $L1_0$ ordered phase which claims $\xi_1^\beta = -\xi_1^\alpha$, $\xi_2^{\alpha\alpha} = \xi_2^{\beta\beta}$ and $\xi_3^{\alpha\beta\beta} = -\xi_3^{\alpha\alpha\beta}$. Hence, the final form of the free energy is given as

$$F^{L1_0} = F(T, \xi_1^\alpha, \xi_2^{\alpha\alpha}, \xi_2^{\alpha\beta}, \xi_3^{\alpha\alpha\beta}, \xi_4^{\alpha\alpha\beta\beta}). \tag{28}$$

Note that the superscript * is omitted from the temperature to avoid unnecessary confusion. Among these five correlation functions, ξ_1^α serves as a Long Range Order parameter (LRO), since it is readily shown from eq. (22) that

$$\xi_1^\alpha = x_A^\alpha - x_A^\beta, \tag{29}$$

while the rest of the correlation functions are Short Range Order parameters (SRO).

When the free energy is minimized with respect to all the correlation functions at a given temperature T,

$$\left.\frac{\partial F^{L1_0}}{\partial\{\xi_m^\delta\}}\right|_T = 0, \tag{30}$$

one obtains the equilibrium state. In the present study, however, we performed a constrained minimization in which only SRO's participate in minimization under a specified LRO at each temperature

$$\left.\frac{\partial F^{L1_0}}{\partial\{\xi_m^\delta\}}\right|_{T,\xi_1^\alpha} = 0. \tag{31}$$

Then, one obtains the Free energy F^{*L1_0} as a function of T and ξ_1^α. The subscript * implies that the original free energy is subject to the constrained minimization. For the latter purpose, we replace LRO ξ_1^α by η, and the resultant function is written as

$$F^{*L1_0} = f(T, \eta). \tag{32}$$

4. Crystal-Glass transition

A common approach to the crystal–glass (CG) transition within phenomenological studies is to describe the free energy in a power series expansion of an order parameter up to the six-th order. This assures the first-order character of the crystal–liquid transition. Mathematically, the present formalism of the free energy given in eq. (32) is not so trivial to ensure the first-order character of the transition. However, previous calculations of the $L1_0$-disorder phase diagrams[22,28,29] guaranteed the first-order character in eq. (32) in many other ways, including the existence of the two phase region, the discontinuity of the order parameter at the transition temperature, and the separation of the transition temperature and the spinodal ordering temperature. We reconfirmed this by representing the free energy as a function of the order parameter η at various temperatures as shown in Fig. 1.[30]

The horizontal axis is the order parameter η, which represents a liquid phase at unity ($\eta = 1$) and a perfect crystal at null ($\eta = 0$). It is noted that unity (null) is generally assigned to a perfect ordered phase (a completely random phase) in the study of order-disorder transition. Hence, we convert η in eq. (32) from ξ_1^α in eq. (29) through $\eta = 1.0 - \xi_1^\alpha$. We interpret the finite value of the order parameter η as the amount of generalized defects including impurities, dislocations, and lattice vibrations that induce breaking of the crystal symmetry and lead to the liquid transition. The specification of a particular kind of defect is not essential in the present study.

One notices the characteristic free energy curve in which

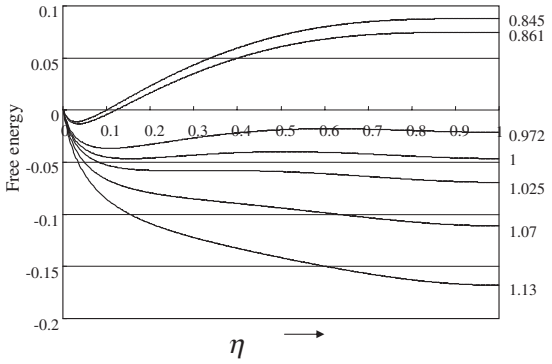

Fig. 1 Free energy $f(\eta, T)$ as a function of the order parameter η at various temperatures indicated on the right hand of the figure. $\eta = 0$ and 1 correspond to a perfect crystal and a liquid phase, respectively. A global minimum appears at $\eta = 0.031$, 0.036 and 0.109 at $T = 0.845$, 0.861 and 0.972, respectively. At $T = 0.972$, a local maximum is found at $\eta = 0.613$. Two global minima coexist at $\eta = 0.153$ and 1.00 at $T = 1.00$. At $T = 1.025$, a local minimum and maximum merge around $\eta = 0.254$ and no local extrema appear above this temperature.[30]

two free energy minima have the same value and a common tangent line has a null slope. The curve is indicated by 1 on the right hand side of the figure. This is the free energy curve, $f(T_t, \eta)$, at the melting point or equilibrium crystal–liquid transition temperature, T_t. The free energy barrier between the two minima suggests the first-order character of the liquid–crystal transition. The number on the right hand side of the figure is the normalized temperature. Note that the temperature T throughout this section is normalized with respect to T_t, and the normalized temperatures of the corresponding free-energy curves are described on the right hand side of Fig. 1.

At temperatures less than $T = 1$, the free energy minimum appears at η closed to null, indicating that the most stable state is a crystal. The deviation of the minima from the null is due to the entropy effect, suggesting that some defects are unavoidable in the crystal at a finite temperature. At the high temperatures greater than $T = 1$, the minima are shifted to $\eta = 1$. There are two characteristic temperatures $T_{\mathrm{L}} = 0.861$ and $T_{\mathrm{H}} = 1.025$ at which the inflection points defined by the following equations appear/disappear in the free energy curve.

$$\frac{\partial^2 f(\eta, T_{\mathrm{L}})}{\partial \eta^2} = \frac{\partial^2 f(\eta, T_{\mathrm{H}})}{\partial \eta^2} = 0. \tag{33}$$

Hence, for the temperature T satisfying $T_{\mathrm{L}} < T < 1$ ($1 < T < T_{\mathrm{H}}$), liquid (crystal) is in a metastable state at a local minimum, while below T_{L} (above T_{H}) liquid (crystal) is unstable. We call these characteristic instability temperatures "spinodal ordering[30]/disordering[25] temperatures" in the case of order-disorder transition.

By following the work of Okamoto,[9] we plot the free energy of $F^{\mathrm{L1}_0} = f(T, \eta)$ as the function of T for various values of η, expressed as $g_\eta(T) = f(T, \eta)$ for the sake of convenience. The results are shown in Fig. 2. $g_{\eta=1}(T) = f(T, \eta = 1)$ expresses the temperature dependency of a liquid free energy. The intersection of $g_\eta(T)$ with $g_{\eta=1}(T)$ defines the T_0 temperature which is regarded as the melting temperature of a defective crystal characterized by the order parameter η. An interesting feature in Fig. 2 is that $g_\eta(T)$ merges to $g_{\eta=1}(T)$ at a critical temperature without an intersection. This implies that the entropy of the defective crystal, given as the slope of $g_\eta(T)$ curve, becomes identical to that of the liquid.

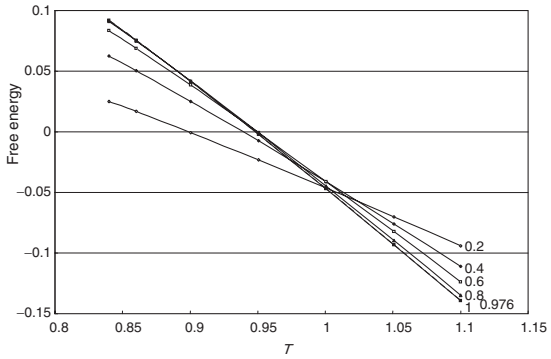

Fig. 2 Free energy curve, $g_\eta(T) = f(\eta, T)$. The intersection of $g_\eta(T)$ with $g_{\eta=1}(T)$ (liquid phase) provides T_0 temperature.

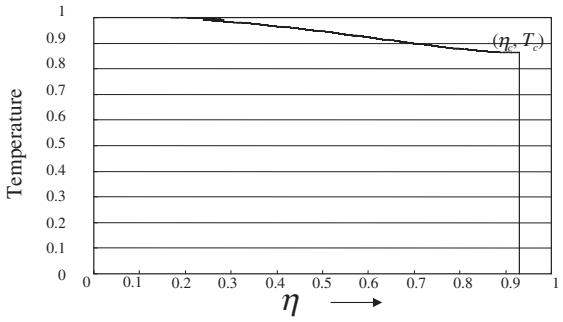

Fig. 3 T_0 diagram indicating a tricritical point which is the glass-transition temperature. The vertical axis corresponds to a normalized temperature.[30]

T_0 temperature is plotted as the function of η in Fig. 3.[30] This is a type of phase diagram but it is more appropriate to call it a T_0 diagram because the equality of the free energy expressed in the diagram does not necessarily guarantee the transition at the equilibrium state. One sees that the melting point deceases with the amount of defects (η). Also, important is the fact that the T_0 curve terminates at a certain critical point $T_{\mathrm{c}} = 0.861$ and $\eta_{\mathrm{c}} = 0.976$, forming a tri-critical point. This is exactly the temperature at which the entropy of the defective crystal becomes identical to that of the liquid, and this is identified as the ideal glass transition temperature. When the defect is further introduced into the crystal at a tri-critical state, the defective crystal transforms into an ideal glass, but upon raising the temperature above T_{c}, the ideal glass becomes a super cooled liquid. One realizes that T_{c} is nothing but T_{L} which was discussed earlier and is characterized as the temperature at which spontaneous loss of the stability begins.

The critical distinction of the physical significance of $T_{\mathrm{c}}(T_{\mathrm{L}})$, however, should be made between an order–disorder transition and a CG transition. For the latter, kinetics plays a crucial role, and the enhanced viscosity virtually blocks the transition to the equilibrium state. The discussions have so far centered around thermodynamic aspects. For the theoretical treatment to be consistent, it is deemed necessary that the kinetics aspects can be described within the same theoretical framework. As mentioned above, the Path Probability Method is the extension of the CVM to the time domain and the CVM inherits advantages in the PPM. We attempted to calculate the time evolution of the order parameters at an aging period following the quenching operation from the liquid state at $T = 1.09$.

Shown in Fig. 4(a)[30] is the aging curve of η at $T = 0.845$ which is below T_{L}. One sees that the value of η decreases with time, finally followed by the transition to crystal. The steady state value of η in the long time limit is confirmed to be the equilibrium η which is independently calculated by the CVM. While for an aging temperature at $T = 0.90$, above T_{L}, as shown in Fig. 4(b),[30] one of two different aging behaviors occur, depending upon the initial deviation of η from the equilibrium value at $T = 1.09$. Imposing an additional chemical potential at the initial time induces such a deviation. With a sufficiently large fluctuation (deviation) tramsition takes place, while for a small deviation, the super-cooled liquid returns to the metastable liquid state. The difference

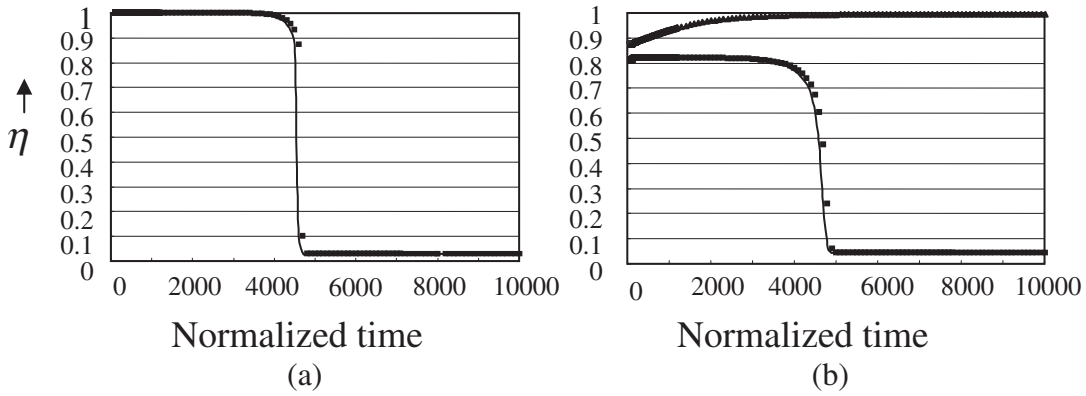

Fig. 4 Time evolution of order parameter η at (a) $T = 0.845$ below T_{L} and (b) 0.90 above T_{L}. The pre-quenching temperature is $T = 1.09$. The horizontal time axis is normalized with respect to spin flipping probability.[30)]

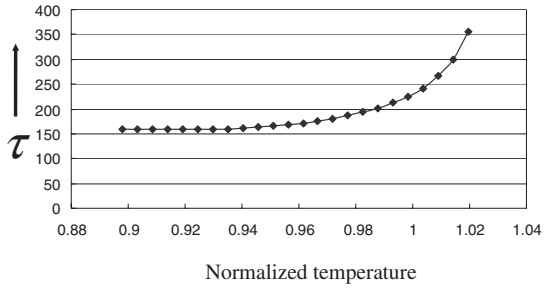

Fig. 5 Temperature dependence of the relaxation time at each aging temperature. The slowing-down takes place near $T_{\mathrm{H}} = 1.025$.

between these two modes of transition at $T = 0.845$ and 0.90 originated from the absence (0.845) or presence (0.90) of the free energy barrier, which is similar to the difference between spinodal ordering and nucleation-growth ordering for the order-disorder transition. In both modes, what is to be emphasized for CG transition is that the time of transition is formidably long on the ordinary lab scale.

Finally, we calculate the relaxation time τ by fitting the aging curve into the following equation,

$$\eta(t) = \eta_{eq} - (\eta_{eq} - \eta_0) \cdot \exp\left(-\frac{t}{\tau}\right). \tag{34}$$

Shown in Fig. 5 is the temperature dependence of the relaxation time when the system is up-quenched to each temperature. One sees that the relaxation time increases with temperature despite the thermal activation event is to be enhanced. This has nothing to do with any atomistic mechanism, but is a natural consequence of the flattening of the free energy surface that leads to a loss of the thermodynamic driving force in the transition. In an order-disorder transition, this is known as a slowing-down phenomenon, and it occurs near the spinodal disordering temperature (transition temperature) for the first order (second order) transitions. In fact, the slowing-down in Fig. 5 occurs near $T_{\mathrm{H}} = 1.025$. To the best of author's knowledge, slowing-down behavior has not been reported in connection with BMG. Examination of the present theoretical result will require further study. In particular, the theoretical investigation of relaxation mechanisms associated with the CG transition is at the core of future study.

The present study demonstrates that a conventional CVM clearly describes the thermodynamic framework of the CG transition. This is quite encouraging to employ the Continuous Displacement Cluster Variation Method (CDCVM) in future studies of atomistic displacement and its correlation with structural and thermal stabilities. Although the application of CDCVM to a realistic alloy system is still at a primitive stage, it is a potential theoretical tool in considering the structural features of BMG, and it may takes us one step further towards analysis of the structural CG transition. The key ability of CDCVM, however, depends on the extent to which we can incorporate topological randomness. This depends crucially on the development of both a sufficient numerical scheme and a powerful computational tool. We emphasize that the advantage of the CVM-based study is that we can investigate the kinetic aspects within the same framework, and thereby perform a consistent study associated with CG transition from thermodynamics to kinetics.

Acknowledgements

The author is grateful to Professor Emeritus T. Takahashi of Hokkaido University for his stimulating discussion and to Mr. Y. Kobayashi for his assistance of preparing the manuscript. The present work is supported by Grant-in-Aid for Scientific Research on Priority Areas, "Materials Science of Bulk Metallic Glasses" from Ministry of Education, Culture, Sports, Science and Technology.

REFERENCES

1) R. Kikuchi: Phys. Rev. **81** (1951) 998.
2) R. Kikuchi: Prog. Theor. Phys. Suppl. **35** (1966) 1.
3) R. Kikuchi and A. Beldjenna: Physica A **182** (1992) 617.
4) R. Kikuchi: J. Phase. Equilibria **19** (1998) 412–421.
5) R. Kikuchi and K. Masuda-Jindo: Comp. Mater. Sci. **14** (1999) 295.
6) H. Uzawa and T. Mohri: Mater. Trans. **42** (2001) 422.
7) H. Uzawa and T. Mohri: Mater. Trans. **42** (2001) 1866.
8) H. Uzawa and T. Mohri: Mater. Trans. **43** (2002) 2185.
9) P. R. Okamoto, N. Q. Lam and L. E. Rehn: *Solid State Physics*, vol. **52**. ed. by H. Ehrenreich (Elsevier Academic Press, San Diego, 1999).
10) C. M. van Baal: Physica, Utrecht **64** (1973) 571.
11) R. Kikuchi and D. de Fontaine: (NBS Publication **SP-496** 1978) 967.
12) D. de Foantine and R. Kikuchi: (NBS Publication **SP-496** 1978) 999.

13) W. Schckley: J. Chem. Phys. **6** (1938) 130.
14) W. L. Bragg and E. J. Williams: Proc. R. Soc. A **145** (1934) 69.
15) R. Kikuchi, J. Chem. Phys. **60** (1974) 1071.
16) T. Mohri and Y. Chen: Mater. Trans. **43** (2002) 2104.
17) Y. Chen, S. Iwata and T. Mohri: Calphad **26** (2002) 583.
18) T. Mohri and Y. Chen: Mater. Trans. **45** (2004) 1478.
19) T. Mohri and Y. Chen: J. Alloys Comp. **383** (2004) 23.
20) T. Mohri, Y. Ichikawa, T. Nakahara and T. Suzuki: *Theory and Applications of the Cluster Variation and Path Probability Methods*, ed. J. L. Moran-Lopez, (Plenum Press, New York, 1996) 37.
21) T. Mohri, Y. Ichikawa and T. Suzuki: J. Alloys Compd. **247** (1997) 98.
22) T. Mohri: *Properties of Complex Inorganic Solids*, ed. A. Gonis, (Plenum Press, New York, 1997) 83.
23) T. Mohri and S. Miyagishima: Mater. Trans., JIM **39** (1998) 154.
24) T. Mohri: Z. Metallkunde **90** (1999) 71.
25) T. Mohri: Modelling Simul. Mater. Sci. Eng. **8** (2000) 239.
26) T. Mohri: *Properties of Complex Inorganic Solid* 2, ed. A. Meike, (Kluwer Academic/Plenum Publishers, 2000) 123.
27) J. M. Sanchez and D. de Fontaine: Phys. Rev. B **17** (1978) 2926.
28) T. Mohri, J. M. Sanchez and D. de Fontaine: Acta Metall. **33** (1985) 1463.
29) T. Mohri, J. M. Sanchez and D. de Fontaine: Acta Metall. **33** (1985) 1711.
30) T. Mohri: submitted to *The Science of Complex Alloy Phases*, Proceeding of TMS 2005 meeting.
31) D. de Fontaine: Acta Metall. **23** (1975) 553.
32) R. J. Glauber: J. Math. Phys. **4** (1953) 294.
33) K. Kawasaki: Phys. Rev. **145** (1966) 224.